Negative extensibility metamaterials: Occurrence and design-space topology

Eduard G. Karpov,* Larry A. Danso, and John T. Klein
Department of Civil and Materials Engineering, University of Illinois at Chicago, 842 W Taylor Street, Chicago, Illinois 60612, USA
(Received 25 May 2017; published 7 August 2017)

A negative extensibility material structure pulls back and contracts when the external tensile load reaches a certain critical level. In this paper, we reveal basic mathematical features of the nonlinear strain energy function responsible for this unusual mechanical property. A systematic discussion leads to a comprehensive phase diagram in terms of design parameters for a simple unit cell structure that provides a panoramic view of all possible nonlinear mechanical behaviors. A negative extensibility region clearly is identified in the diagram. The sought property is seen to be rare, occurring only for a very narrow range of the design parameters. Nonetheless, due to the simplicity of the studied structure we suggest that the negative extensibility should be a more common phenomenon than previously thought. It can appear in simple *bistable* cells made of only several linearly elastic links, although at some peculiar combinations of their properties. These bistable unit cells can be used to design periodic mechanical metamaterials whose examples are shown as well as innovative architectural metastructures.

DOI: 10.1103/PhysRevE.96.023002

I. INTRODUCTION

Mechanical and structural metamaterials [1–18] are associated with the reversal of basic mechanical properties in quasistatic loading cycles. In particular, auxetic metamaterials [6–9] demonstrate a negative Poisson ratio, whereas for origami-based metamaterials [10–12], a negative Poisson ratio and negative bending and twisting stiffnesses can be expressed analytically or observed numerically. Nicolaou and Motter [15,16] also showed the possibility for engineered materials with a longitudinal negative compressibility or extensibility property that would contract in the direction of the applied tensile load, Fig. 1. The same authors suggested that such a contraction may occur only in an abrupt manner because of the destabilization of the materials internal structure at the unit cell level when the external load exceeds some threshold value. Chen and Karpov [17] discussed an essential *bistable* nature of negative extensibility structures and metamaterials, whose forward and reverse transitions can be viewed as a polymorphic phase transformation on the microscopic scale. Such a solid-to-solid condensation process is reminiscent of a superelastic phase transition, and it is accompanied by an abrupt energy release in the structure. Two microstructural polymorphs exhibit different stiffnesses, and therefore two different stable states of equilibrium are possible for the same external load. This behavior implies a hysteretic response of the material to periodic loads [15–17].

A representative potential or strain energy function written for a repetitive unit cell structure of a negative extensibility metamaterial must possess rather exotic mathematical properties. In this paper, we discuss a path toward practical negative extensibility metamaterials via the study of macroscopic structural composites—periodical arrangements of unit cells featuring bistable mechanical hysteresis. These cells are made of *linearly* elastic springs and bars only, and they can have their own interesting applications as mechanical actuators, earthquake and explosion impact superdampers, or reconfigurable civil infrastructure components. Furthermore, once important mathematical criteria are understood and many practical examples of these structural metamaterials are demonstrated in the first place, the knowledge gained will facilitate the design of negative extensibility in materials on the atomic scale.

From the known cases [15–17] it is clear that a representative (unit) cell of a periodic negative extensibility metastructure may have several degrees of freedom (DOF), including at least one internal degree of freedom, even for the case of chainlike models. A systematic stability analysis of such unit cells featuring an essential material or/and geometrical nonlinearity, leading to a bistable hysteretic response, is highly challenging.

In this paper, we rely on geometrical nonlinearity only and discuss an approach to elucidate many necessary features of the potential energy function and to provide practical guidelines toward a negative extensibility phenomenon in a macroscopic metastructure made of linearly elastic elements only. A practical mechanical metamaterial would employ this metastructure as a main phase as well as damping elements since the negative extensibility transitions are known to be accompanied by the release of large amounts of kinetic energy [17]. Thus, we focus on simple bistable unit cells that can potentially be arranged in periodic arrays and that can be made using only the following nonbuckling element types: (a) linear springs or strings allowing for the large deformation described by the engineering strain,

$$\varepsilon = \frac{l - l_0}{l_0}, \tag{1}$$

(b) linear elastic bars at moderate deformation measured with the Green's strain,

$$\varepsilon_G = \frac{l^2 - l_0^2}{2l_0^2}, \tag{2}$$

and (c) rigid pivoted links with no strain. The potential energy of the deformation of the spring and bar elements, respectively, gives

$$\pi_s = \frac{k_s}{2} l_0^2 \varepsilon^2 = \frac{k_s}{2}(l - l_0)^2, \tag{3}$$

$$\pi_b = \frac{k_b}{2} l_0^2 \varepsilon^2 \approx \frac{k_b}{2} l_0^2 \varepsilon_G^2 = \frac{k_b}{8 l_0^2}\left(l^2 - l_0^2\right)^2, \tag{4}$$

*Corresponding author: ekarpov@uic.edu

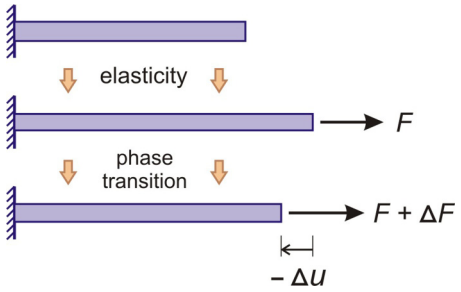

FIG. 1. Concept of the longitudinal negative extensibility. Elastically deformed material contracts abruptly in the direction opposite to the force load when the load reaches a critical value inducing a polymorphic phase transition. Effective elastic modulus and mechanical extensibility $(-\Delta u/\Delta F)$ at a constant temperature are negative around the transition point.

where k, l_0, and l are the stiffness and the relaxed and deformed lengths of the elements. The bar's stiffness is $k_b = EA/l_0$ in terms of its Young's modulus E and cross-sectional area A. Equation (4) represents the only approximation adopted in the analysis, and it is good at moderate strains in the bars (0.05) because $\varepsilon_G = \varepsilon + \varepsilon^2/2$.

The strain energies (3) and (4) will lead to quartic (bistable) potentials for the structure's representative unit cells, whose mathematical stability analysis is tractable. In the simplest case of the Fig. 2(a) structure with one independent degree of freedom, we may write the total potential energy as

$$\Pi = \frac{k_b}{4(L^2+H^2)}(u^2 - 2Hu)^2 + \frac{1}{2}k_s u^2 - Fu, \qquad (5)$$

where k_b and k_s are the bar and spring stiffnesses, respectively. This expression can be written in a dimensionless form

$$U = x^4 - ax^3 + bx^2 - fx, \qquad (6)$$

$$f = \frac{4(L^2+H^2)}{H^3}\frac{F}{k_b}, \quad U = \frac{f}{H}, \quad x = \frac{u}{H},$$

$$a = 4, \quad b = 4 + \frac{2(L^2+H^2)k_s}{k_b H^2}. \qquad (7)$$

A similar potential energy expression (6) can also be written for the Fig. 2(b) structure, although using its own dimensionless parameters,

$$f = \frac{L^2+H_2^2}{H_1^3(1+\gamma)}\frac{F}{k_2}, \quad U = \frac{f}{H_1}, \quad x = \frac{u}{H_1},$$

$$a = \frac{H_2+\gamma H_1}{H_1(1+\gamma)}, \quad b = \frac{H_2^2+\gamma H_1^2}{H_1^2(1+\gamma)}, \qquad (8)$$

where $\gamma = \frac{L^2+H_2^2}{L^2+H_1^2}\frac{k_1}{k_2}$. In Eqs. (6)–(8), the dimensionless load f is an external *control* parameter, the dimensionless displacement x is a *state* parameter describing the state of deformation, and the coefficients a and b are the *system* or *design* parameters. This terminology is typical for catastrophe theory [19–21] where design parameters of this type, though, may serve the role of control parameters since they define a desired system behavior. Note that the Fig. 2(a) structure has only one independent design parameter since the value a cannot vary in (7). A discussion of the Fig. 2(c) structure and other examples leading to the potential energy form (6) can be found in Ref. [22]. A *phase diagram* of the generic system governed by (6) can be constructed for the system parameters a and b, and it is shown in Fig. 3(a). Here, three basic types of the mechanical response are possible. One of them is monostable and two are *bistable*—when two stable equilibrium configurations are possible for a same load. The bistable (hysteretic) response can be either *structural superelasticity* or *structural superplasticity* [22] depending on whether the initial configuration is recovered upon load removal. The term superplasticity implies that a full recovery of the overall (structural) plastic deformation is still possible upon load reversal, see Fig. 3(b).

The bottom line in the phase diagram, Fig. 3(a), represents the onset of bistability because all designs above this line are bistable and all those below are monostable. This line is a locus of points $\{a,b\}$ that represent simultaneously a mechanical equilibrium, destabilization (zero stiffness), and an undulation point or cusp singularity [22–21] of the potential,

$$U_x' = U_{xx}'' = U_{xxx}''' = 0: \quad 3a^2 - 8b = 0. \qquad (9)$$

The upper curve in the Fig. 3(a) diagram represents designs where the reverse destabilization and transition $B \to A$ occurs at a zero load. These design points must satisfy the condition,

$$U_x' = U_{xx}'' = 0 \ \wedge \ f = 0: \quad 9a^2 - 32b = 0. \qquad (10)$$

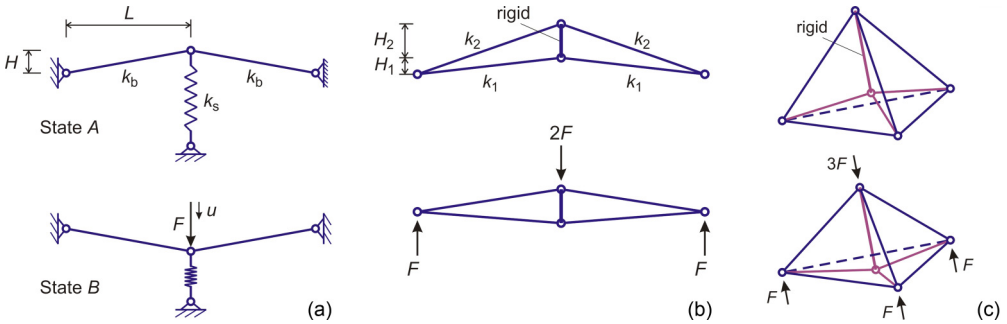

FIG. 2. Examples of bistable structures with one independent degree of freedom. Parameters k are linear stiffnesses of the spring or bar elements.

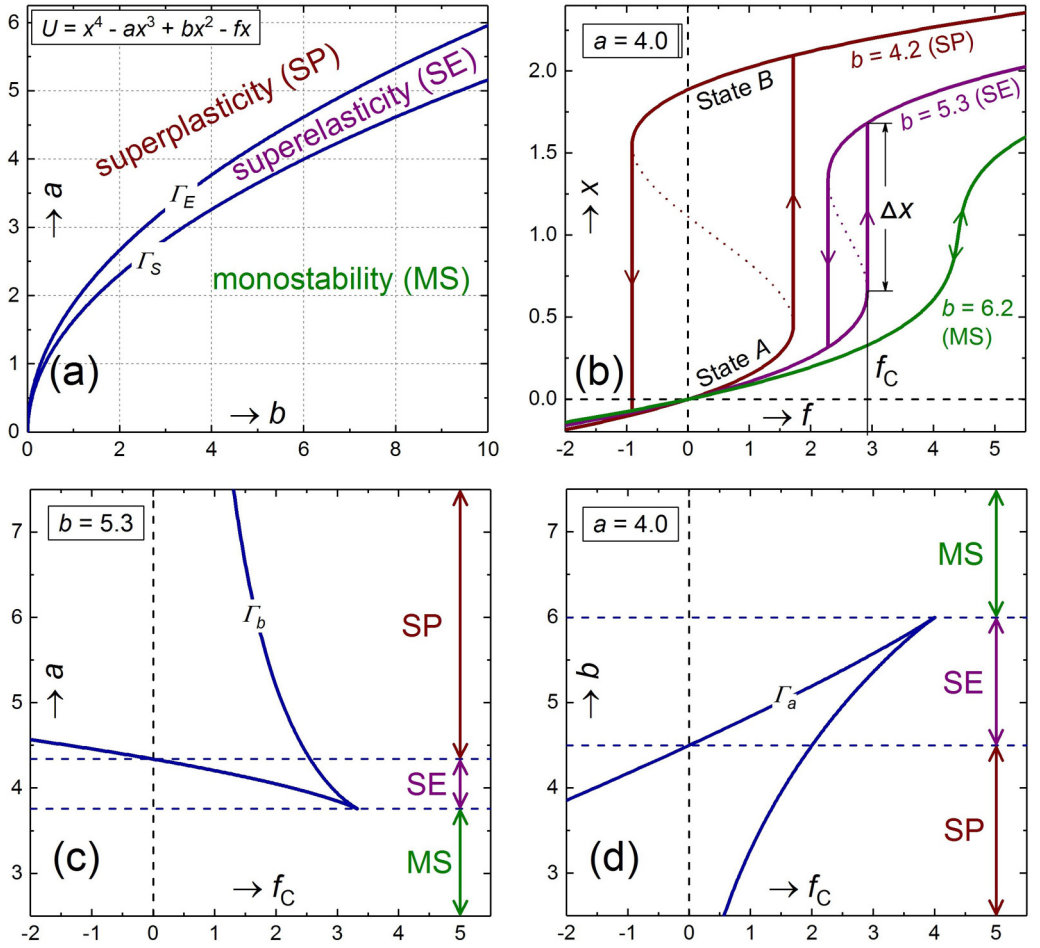

FIG. 3. (a) Phase diagram of the generic system governed by the quartic potential $U = x^4 - ax^3 + bx^2 - fx$. (b) Three possible types of the mechanical response: structural monostability (MS) or usual geometrical nonlinearity, bistable superelasticity (SE), and bistable superplasticity (SP) when the recovery of structural deformation requires load reversal. Switching between states A and B occurs at a critical load $f = f_C$. Superelastic strain due to the transition ε_{SE} is proportional to Δx. (c) and (d) Stability diagrams showing values of the critical forces f_C at specific values of the system parameters a and b.

The *stability diagrams* of Figs. 3(c) and 3(d) show the critical loads $f = f_C$ at which structural destabilization will occur at given system parameters. The curves shown were plotted parametrically by fixing either b or a and using x as a running variable,

$$U'_x = U''_{xx} = 0: \begin{cases} f_C = x(b - 2x^2), & a = \frac{b}{3x} + 2x, \\ f_C = x^2(3a - 8x), & b = 3x(a - 2x). \end{cases} \tag{11}$$

As can be seen, the Fig. 3 diagrams provide a panoramic view of all possible basic types of mechanical behavior in the bistable systems of the Fig. 2 type. These diagrams also enable the design of a specific desired behavior as well as magnitudes of the critical loads associated with the forward and reverse transitions of the system. We note that negative extensibility is not observed yet in the simplest bistable cells as in Fig. 2, which can be described by the potential (6) and the Fig. 3(a) phase diagram. Apparently, negative compressibility requires a more complex form of bistability involving a greater number of independent degrees of freedom per unit cell.

Nicolaou and Motter [15] and Chen and Karpov [17] provided good reasoning that the sought negative extensibility behavior must arise from at least one or more additional independent *internal* degrees of freedom in a representative unit cell of the metamaterial. In this paper, we suggest that systematic studies of such bistable unit cells could employ analytical reasoning similar to Eqs. (1)–(7), strengthened by the numerical solution of nonlinear algebraic equations of the type (8)–(10). We will derive a generic potential energy form for a class of bistable structures with two independent degrees of freedom, including one internal degree of freedom, followed by a phase diagram derivation and a demonstration of the negative extensibility property at a certain combination of the system parameters.

More importantly, using this semianalytical approach we will show that the negative extensibility is probably a more common phenomenon than previously thought. It may occur for rather simple structures made of several linear elastic links although at some rare combinations of their physical parameters.

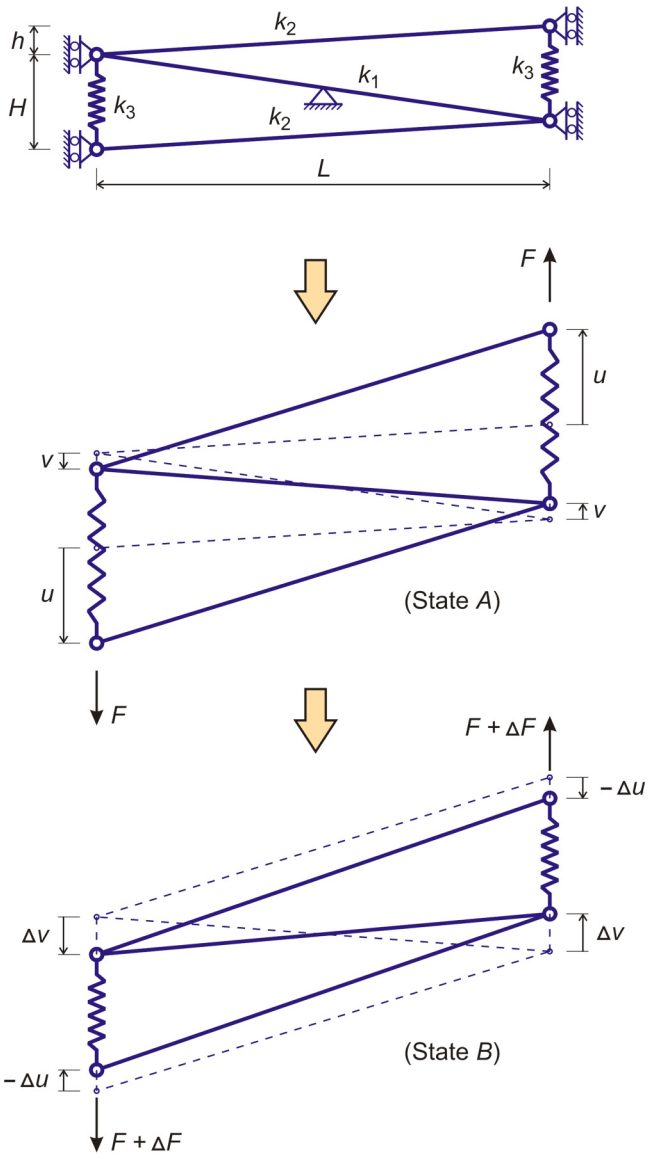

FIG. 4. Negative extensibility phenomenon in a five-element bistable structure (unit cell) with linearly elastic members and two independent degrees of freedom, the vertical displacements u and v. L, H, and h are dimensions of the unloaded structure at $F = 0$, and k_i's are linear stiffnesses of the bar and spring elements. The structure contracts in the direction of the applied load when the latter reaches a critical value that destabilizes the structure and induces the transition. This transition is associated with the intermittent rotation of the middle bar pulling back on the top and bottom bars of the structure. The negative superelastic strain due to the $A \to B$ transition is $\varepsilon_{SE} = -2\,\Delta u/(H + h)$.

II. NEGATIVE EXTENSIBILITY PHENOMENON

Consider a five-element structural unit cell of the Fig. 4 type, composed of three inclined bars at moderate deformation and two vertical springs allowing for large elongations. Possible periodic arrangements of such a unit cell in mechanical metamaterials are shown further below in Fig. 10.

Using the engineering strain (1) for the springs k_3 and the Green's strain (2) for the bars k_1 and k_2, we can write their strain energies,

$$\pi_1 = \frac{2k_1}{L^2 + (H - h)^2} v^2 (v - H + h)^2, \tag{12}$$

$$\pi_2 = \frac{k_2}{8(L^2 + h^2)} (u + v)^2 (u + v + 2h)^2, \tag{13}$$

$$\pi_3 = \frac{k_3}{2} (u - v)^2. \tag{14}$$

The total potential energy of the Fig. 4 structure is

$$\Pi = \pi_1 + 2(\pi_2 + \pi_3 - Fu), \tag{15}$$

In order to minimize the number of independent system parameters, we may rewrite the potential (15) in terms of the dimensionless quantities,

$$U = a(x + y)^2 (x + y + 2s)^2 + by^2 (y - 1 + s)^2 + (x - y)^2 - 2fx, \tag{16}$$

$$U = \frac{\Pi}{k_3 H^2}, \quad f = \frac{F}{k_3 H}, \quad x = \frac{u}{H}, \quad y = \frac{v}{L},$$
$$a = \frac{k_2}{4k_3} \frac{H^2}{L^2 + h^2}, \quad b = \frac{2k_1}{k_3} \frac{H^2}{L^2 + (H - h)^2}, \quad s = \frac{h}{H}. \tag{17}$$

By analogy with Eq. (6), the dimensionless force f is the control parameter, x and y are two independent state parameters, and a, b, and s are the system (design) parameters.

Interestingly, numerical minimization of the potential (16) at certain combinations of the system parameters can provide a pinched hysteresis response with a sought negative extensibility transition. A particularly large contraction at an increasing tensile load was seen at $a = 0.0665$, $b = 5.21$, and $s = 0$ when the $A \to B$ state switching occurred at the critical load $f_C = 1.33$, see Fig. 5. The figure shows a numerical solution of Eq. (16) using a gradient method where the force parameter f was varied from 0.0 to 1.7 and backward with a step ± 0.001, and the trial solution $x_0 = y_0 = 0.001$ was set initially. Solutions from previous steps were used as trial solutions at further iterations of the force parameter.

We explored the Fig. 4 type structures of different skewnesses $s = h/H$ using the analysis to follow and found that the maximal magnitude of the negative extensibility effect has a weak dependence on s in the range from -0.5 to 0.5 and it is better pronounced in *rectangle*-shaped cells. For a concise discussion, we therefore set $s = h = 0$ in (16) and (17) and write the final form of the potential in question,

$$U = a(x + y)^4 + b(y^2 - y)^2 + (x - y)^2 - 2fx,$$
$$a = \frac{k_2}{4k_3} \frac{H^2}{L^2}, \quad b = \frac{2k_1}{k_3} \frac{H^2}{L^2 + H^2}, \tag{18}$$

The Fig. 5 behavior is qualitatively similar to the negative extensibility observed in some hypothetical atomic systems governed by much more complex potentials [15–17]. We point out, though, the existence of a secondary (superelastic type) hysteresis at higher loads not mentioned in the earlier publications. We will see below that it should be characteristic for all

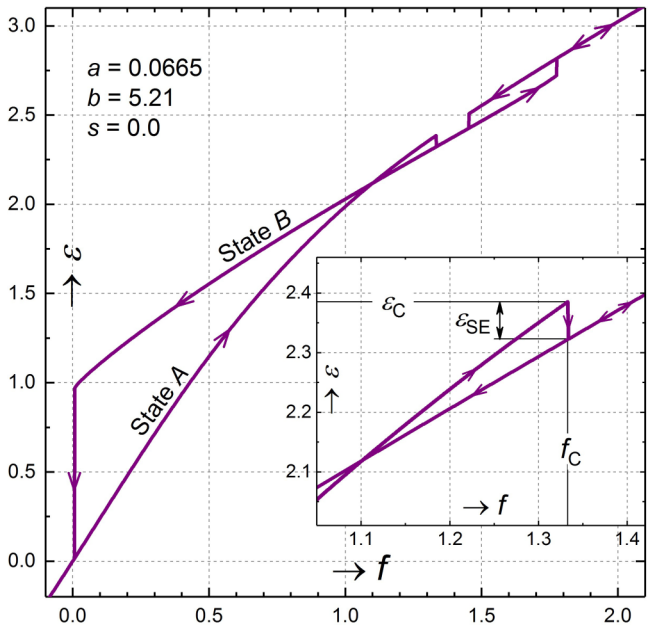

FIG. 5. Load-unload cycle of the Fig. 4 bistable structure governed by the potential (16) or (18) showing a pinched hysteresis and a negative extensibility transition at the critical force $f_C = 1.33$ or critical strain $\varepsilon_C = 2.385$. The negative superelastic strain solely due to the transition $\varepsilon_{SE} = -0.063$. A secondary hysteresis also exists at the higher loads. States A and B are two structural *polymorphs* with different stiffnesses. The overall path of load-induced switching between the states is $A \to B \to A \to B \to A$.

bistable structures with a negative extensibility transition, and therefore their overall path along the switching equilibrium states could be $A \to B \to A \to B \to A$ in larger amplitude load cycles. Also, simplicity of the potential (18) will enable us to determine an entire range of the system parameters a and b leading to this remarkable mechanical behavior.

III. STRUCTURAL DESTABILIZATION AND BIFURCATION POINTS

Stationary points of the scalar potential (18) are defined by the simultaneous conditions,

$$U'_x = 0: \quad g_1(x,y,f,a,b) = x - y + 2a(x+y)^3 - f = 0, \tag{19}$$

$$U'_y = 0: \quad g_2(x,y,a,b) = y - x + 2a(x+y)^3 + by(y-1)(2y-1) = 0, \tag{20}$$

which correspond to a mechanical equilibrium of the structure. We will refer to these conditions as the *equilibrium set* conditions. Specific equilibrium states $\{x,y\}$ will depend on the combinations of the control and system parameters $\{f,a,b\}$. The equilibrium set is an intersection of the hypersurfaces g_1 and g_2.

Structural destabilization and switching to a new stable equilibrium configuration occurs in a snap-through action when the external load reaches some critical value of f_C. Mathematically, this corresponds to an *inflection point* singularity on the potential (18) or a *saddle node* bifurcation in the solution space. A necessary mathematical condition for an inflection point can be written in terms of the determinant of the Hessian matrix of second-order derivatives of the potential (18) [19–21],

$$\det H = \begin{vmatrix} U''_{xx} & U''_{xy} \\ U''_{yx} & U''_{yy} \end{vmatrix} = U''_{xx}U''_{yy} - U''_{xy}U''_{yx} = 0:$$

$$g_3(x,y,a,b) = 24a(x+y)^2 + b(6y^2 - 6y + 1) \times [1 + 6a(x+y)^2] = 0. \tag{21}$$

The condition (20) replaces $U''_{xx} = 0$ used in (11) for the analysis of structures with one independent degree of freedom. In an immediate vicinity of a limit point, the structure is in equilibrium, and therefore the criterion for an inflection point (structural destabilization) is the following:

$$g_1(x,y,f_C,a,b) = g_2(x,y,a,b) = g_3(x,y,a,b) = 0. \tag{22}$$

The locus of all the limit points $\{f_C,a,b\}$ satisfying (22) is a three-dimensional (3D) surface $\Phi_L(f_C,a,b) = 0$ that we may call the *limit set*. Also, the term *bifurcation set* from the catastrophe theory [19–21] could be used since $\Phi_L(f_C,a,b) = 0$ contains absolutely all bifurcation points of the potential (18) including the higher-order pitchfork bifurcations discussed below. Using the term bifurcation set, one should be aware of a possible confusion; indeed, a bifurcation point in structural analysis is where an equilibrium solution splits rather than jumps.

In a practical sense, the criterion (22) can provide values of the critical (destabilizing) loads f_C for any specific system parameters a and b. Thus, geometry of the limit set $\Phi_L(f_C,a,b) = 0$ is interesting, although difficult to realize for 2DOF systems, and we will discuss it in more detail in Sec. II B. Note that the limit set geometry for the 1DOF potential (6) was well represented by the stability diagrams in Figs. 3(c) and 3(d) showing its two plane cross sections at some fixed values of a and b.

When the system parameters a and b are varied in a design process, a stable equilibrium solution $\{x,y\}$ of the equilibrium equations (18) may lose uniqueness at a point of *supercritical pitchfork bifurcation* [23] and split into two stable and one unstable solutions. For the systems with one degree of freedom, this occurred at the *cusp points* (9) within limit set (11) of the potential (6), and these points satisfied the additional condition: $U'''_{xxx} = 0$, see Ref. [22] for more details. We suggest that such a condition should generally apply to an internal degree of freedom responsible for the destabilization. For the Fig. 4 structure, this degree of freedom is the rotation of the middle bar k_1 on the plane of the structure, and therefore, we will require

$$U'''_{yyy} = 0: \quad g_4(x,y,a,b) = 24a(x+y) + 12b(2y-1) = 0. \tag{23}$$

Thus, the criterion for a cusp point (solution splitting) can be written as the following:

$$g_1(x,y,f,a,b) = g_2(x,y,a,b) = g_3(x,y,a,b) = g_4(x,y,a,b) = 0. \tag{24}$$

The locus of all the cusp points $\{a,b\}$ satisfying (24) is a plane curve $\Gamma_S(a,b) = 0$, and we will call it the *cusp set*. Individual points $\{a,b\}$ of the cusp set are independent of the load f because a supercritical pitchfork bifurcation is an outcome of design modification rather than the loading change as it was for the saddle-node bifurcations (22). Availability of a nontrivial solution to the equation set (24) in the form of an actual plane curve $\Gamma_S(a,b) = 0$ will indicate that the structure can be bistable as in principle. One may further assume that the curve Γ_S itself should represent a boundary of the bistability region in the ab-parameter design space, similar to the 1DOF systems, see Eq. (9) and Fig. 3(a). However, using the Fig. 4 structure as an example, we will later see that the true onset of bistability in 2DOF systems may correspond to a condition weaker than (24).

A. Limit set geometry

For the potential (18), it was possible to derive a unique analytical solution for the limit set equations (22) in terms of $f_C = f_C(y,b)$, $a = a(y,b)$, and $x = x(y,b)$ via algebraic substitution, see Eqs. (A1) and (A2) in the Appendix. Therefore, using y as a varying parameter, we may draw a parametric plane curve $\Gamma_b(f_C,a) = 0$ to represent the (f,a)-*stability diagram* for a given fixed value of b. Two examples of it are shown in Figs. 6(a) and 6(b). Such a diagram shows a relationship between the system parameter a and the critical loads f_C upon which the switching between two stable equilibrium configurations would occur. It also represents a planar cross section of the limit set $\Phi_L(f_C,a,b) = 0$ at the fixed value of b.

It is also interesting to see a cross section of the set $\Phi_L(f_C,a,b) = 0$ for a fixed value of a, leading to the (f,b)-*stability diagram*. However, for the potential (18), it is not possible to derive an exact algebraic solution for (22) in terms of $f_C = f_C(y,a)$ and $b = b(y,a)$, and we employed a numerical Newton-Raphson iterative procedure for the nonlinear equations set (22) at various instances of y. It was possible to obtain smooth curves when y varied from 0.22 to 0.78 with a step of 0.002. Solutions from previous steps were used as trial solutions for each next iteration of y. Two examples of the curve $\Gamma_a(f,b) = 0$ are shown in Figs. 6(c) and 6(d) for $a = 0.04$ and 0.0665. Noteworthy, each of these curves contains two cusp points and a local maximum. Therefore, a range of the system parameters a and b exists at which we can observe switching between states A and B four times (in the manner of $A \to B \to A \to B \to A$) at four different values of the critical force f_C during a *single* load-unload cycle. An example of such a mechanical response was shown earlier in Fig. 5.

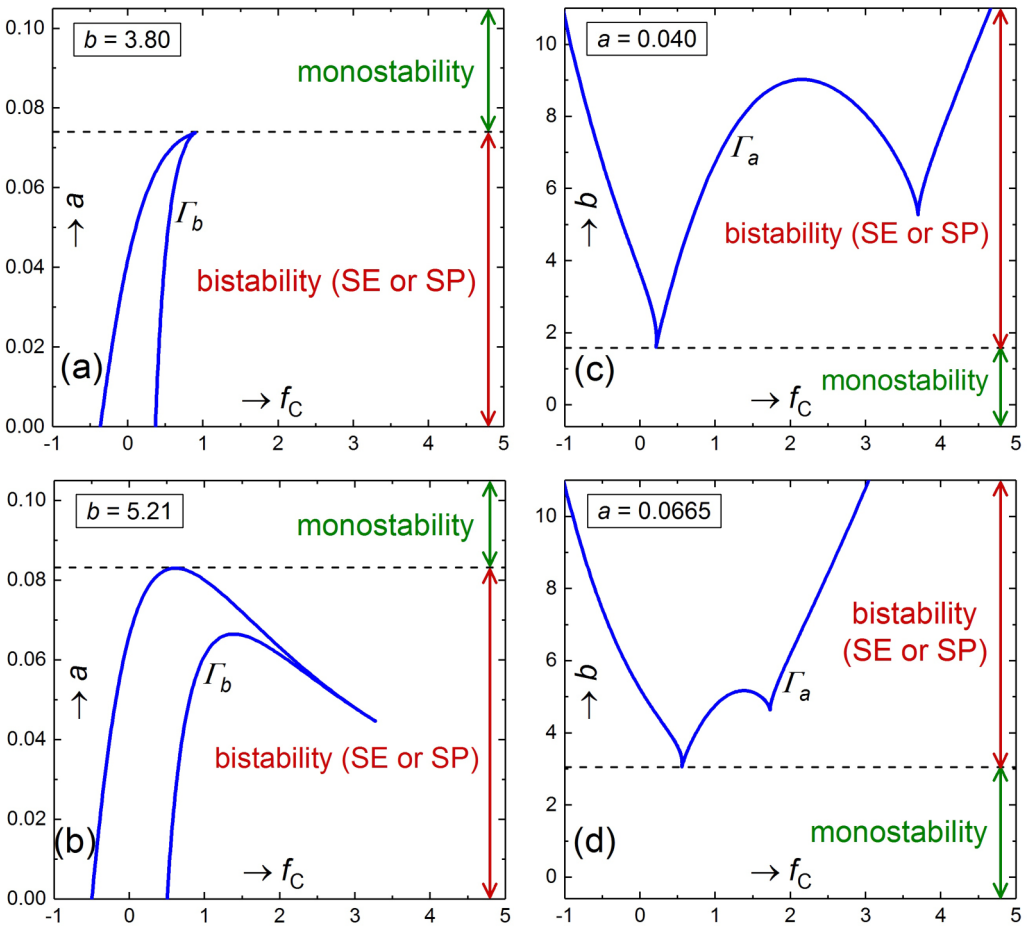

FIG. 6. Stability diagrams of the Fig. 4 bistable structure governed by the potential (18). Up to four critical forces f_C are possible for some selections of the system parameters a and b. The bistable response can be either SE when the original configuration is fully restored upon load removal or SP when the recovery requires load reversal by analogy with Fig. 3.

B. Negative extensibility behavior

The most important consequence of the double cusp points mentioned in the previous section is the possibility for a pinch hysteresis required for the negative extensibility behavior. Indeed, values a and b can be selected so that the first transition $A \rightarrow B$ leads to a contraction of the structure in the direction of the applied load, see Fig. 5. Availability of the four-step transition during a load-unload cycle for an elastic structure seems to be a common feature to accompany the negative extensibility behavior.

C. Bistability region clarified

As was mentioned earlier in Sec. II A, a single stable solution to the equilibrium equations may split into two stable and one unstable solutions at a cusp point in the ab-parameter space. For such a special point, four simultaneous conditions (24) must be satisfied. The locus of all the cusp points is the *cusp set*, a plane curve $\Gamma_S(a,b) = 0$. It was possible to get a smooth numerical solution of Eqs. (24) for the potential (18) in terms of a, f, x, and y, depending on the parameter b with the Newton-Raphson method applied to (24) for each specific value of b. The resultant dependence $\Gamma_S(a,b) = 0$ is shown in Fig. 7, where b was varied from 0 to 6.5 with a step of 0.02.

Some important disclaimers have to be made prior to adopting the curve $\Gamma_S = 0$ in Fig. 7 as the onset of bistability. From the bifurcation set geometry discussed in the previous section, we may see that, for some values of b, the bifurcation curve is bent down in a "beak" shape, see Fig. 6(b). This

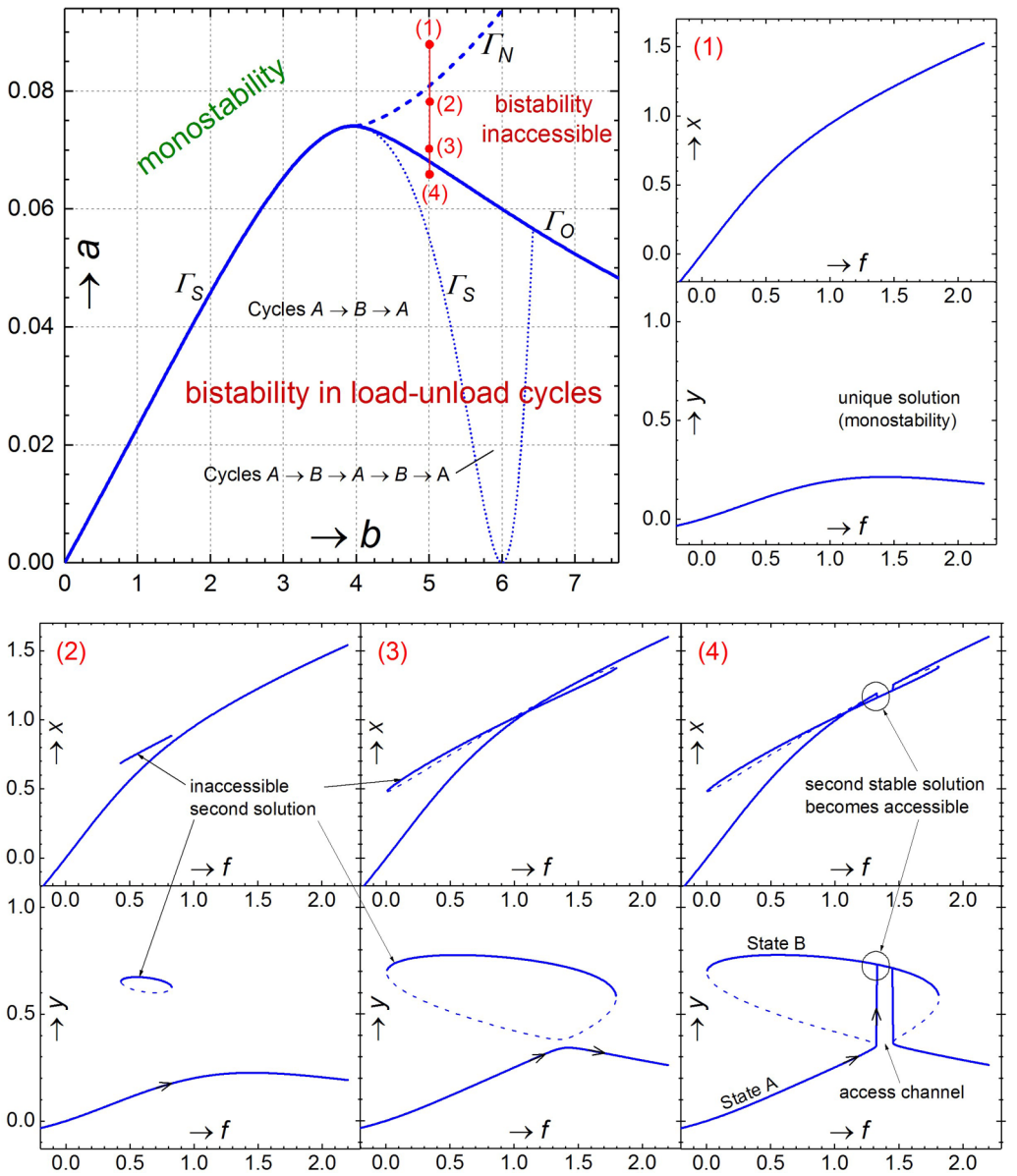

FIG. 7. Principal regions of mono- and bistability in the space of design parameters of the potential (18) and a graphical explanation of the second stable solution's nucleation and accessibility change with a decrease in parameter a along the line 1-2-3-4. The second stable solution becomes accessible when the new stable-unstable solution loop on the fy plane coalesces with the old solution forming an access channel. The lines Γ_S, Γ_N, and Γ_O represent the locus of the cusp, nucleation, and coalescence points of the potential (18) accordingly.

indicates that the structure may start to demonstrate a bistable behavior (with a decrease in a) *earlier* than the cusp point. Indeed, it is sufficient that the value of a is found lower than the local maximum on the upper branch of the $\Gamma_b(f_C,a) = 0$ curve in Fig. 6(b). At this point, another pitchfork bifurcation occurs leading to solution splitting into two stable and one unstable configurations. However, the second stable solution nucleates as shown in Fig. 7 to coexist independently in a neighbor region of the solution space inaccessible by the loading of the Fig. 4 type. It can only be accessed by applying certain coordinated loads to all four nodes of the structure, which is not practical. The points of nucleation of the inaccessible second stable solutions can be determined as those corresponding to the local maximum on the upper branch of the curve $\Gamma_b(f_C,a) = 0$ in Fig. 6(b), and they are plotted in the Fig. 7 diagram as the dashed line Γ_N.

As can be seen from the Fig. 7 plots, this second solution, in a pair with an unstable solution, forms a loop on the fy-plane section of the solution space. This loop grows with a decrease in a, until it coalesces with the first stable solution, followed by formation of an access channel between them. This channel makes state B accessible in a usual load-unload cycle. The locus of the coalescence points on the ba plane can be determined from the local maximum on the lower branch of the curve $\Gamma_b(f_C,a) = 0$, and they are plotted in the Fig. 7 diagram as the dashed line Γ_O.

The line of coalescence points Γ_O merges with the cusp curve Γ_S at $b = 4$ forming a single continuous boundary of the region of the true physical bistability, observable in load-unload cycles of the Fig. 4 structure. This boundary is shown as the continuous solid line in the Fig. 7 diagram. In accordance with the stability diagrams of Fig. 6, the dotted section of the cusp curve Γ_S below the line Γ_O separates the region of the fourfold switching cycles $A \to B \to A \to B \to A$. We will narrow it to a region of the negative extensibility behavior in the section to follow.

IV. STRUCTURAL PHASE DIAGRAM

The plot of Fig. 7 is a prototypical phase diagram of the structure showing a boundary between two principal types of structural behavior, bistability and monostability, in the design space. We may now further clarify the behavior subtypes within the bistability region. Since the negative critical forces exist in Fig. 6 stability diagrams, the superelastic (reversible on load removal) and superplastic responses should be distinguished, and we saw a negative extensibility response of the structure in the Fig. 5 plot. Thus, two more boundary

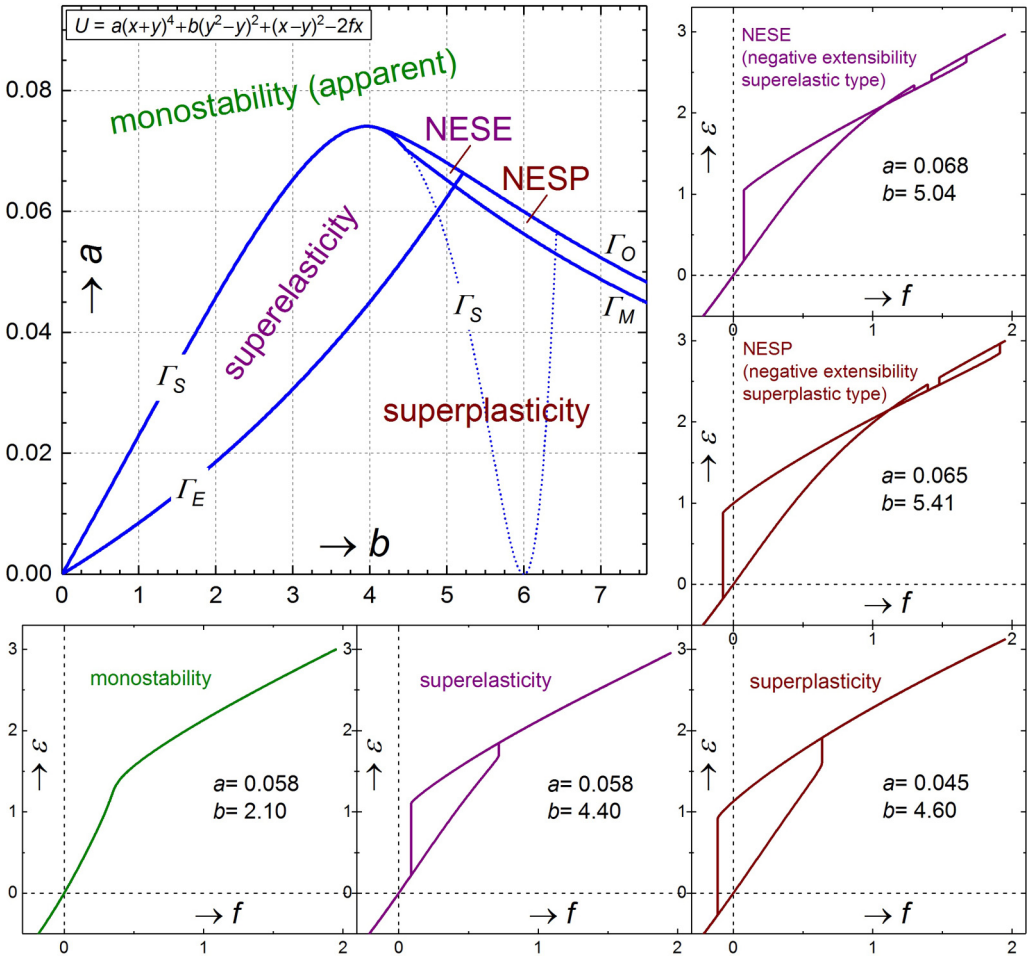

FIG. 8. Phase diagram of the Fig. 4 structure and all mechanical systems governed by the potential $U = a(x + y)^4 + b(y^2 - y)^2 + (x - y)^2 - 2fx$. The most interesting behavior is the NESE in a small region of the design space bounded with the curves Γ_O, Γ_M, and Γ_E. The region of the NESP is somewhat larger.

lines should be added to the Fig. 7 diagram in the region of bistability to complete a structural phase diagram. A region of the negative extensibility behavior of superelastic type (NESE) will be our primary interest as leading to the most interesting mechanical metamaterial applications.

The *elasticity boundary* showing the onset of superelastic behavior when the structure recovers its original configuration upon load removal can be determined from the condition that the critical force f_C at the corresponding destabilization point (22) is equal to zero,

$$g_1(x,y,0,a,b) = g_2(x,y,a,b) = g_3(x,y,a,b) = 0. \quad (25)$$

A Newton-Raphson procedure was used to solve these equations for a, x, and y at each particular value b, which was varied from 0 to 5.21 with a step of 0.01. Solutions from the preceding values of b were used as trial solutions for the successive values of b. The result is a relationship between parameters a and b given by the curve $\Gamma_E(a,b) = 0$ in Fig. 8.

We may now determine the *negative extensibility boundary* or metastructure behavior boundary showing the onset of the most interesting bistable behavior when the structure contracts upon the tensile load increase as a result of the first transition in the cycle $A \to B \to A \to B \to A$. The formal condition to determine this boundary is the following: the transition $A \to B$ can give a large rotation to the middle bar k_1 of the structure, see Fig. 4, whereas the overall height of the structure must *not* change. We can write this conditionx as the following:

$$g_1(x_A,y_A,f,a,b) = g_2(x_A,y_A,a,b) = g_3(x_A,y_A,a,b) = 0$$
$$\wedge g_1(x_B = x_A, y_B, f, a, b) = g_2(x_B = x_A, y_B, a, b) = 0, \quad (26)$$

where x_A and y_A are the values of state parameters x and y in configuration A right before the switching and x_B and y_B are their values right after the switching. These five simultaneous equations can be solved numerically with the Newton-Raphson method for a, f, x_A, y_A, and y_B at a fixed value of b. Varying b from 4.5 to 7.5 with a step of 0.01 gives a relationship between a and b shown as the curve $\Gamma_M(a,b) = 0$ in Fig. 8. As can be seen, the interesting region of the NESE is bound with the lines Γ_O, Γ_E, and Γ_M. The continuation of this region into superplasticity is denoted on the phase diagram as the negative extensibility of superplastic (NESP) type. The NESP behavior may also find interesting applications in mechanical shape-memory systems, thermomechanical actuators, and impact dampers, alongside the NESE.

Finally, we look more closely onto the negative extensibility region and draw the *contour lines* to represent a *relative intensity* of the NESE effect,

$$I_{\mathrm{NESE}} = \frac{\varepsilon_{\mathrm{SE}}}{\varepsilon_C}, \quad (27)$$

where ε_C is the critical elastic strain and $\varepsilon_{\mathrm{SE}}$ is the negative superelastic strain at the NESE transition $A \to B$, see the Fig. 5 inset. This parameter describes the relative contraction of the structure due to the transition. Noting that the effect intensity is zero along the curve $\Gamma_M(a,b) = 0$, we can relate the dimensionless displacements right before (x_A) and right

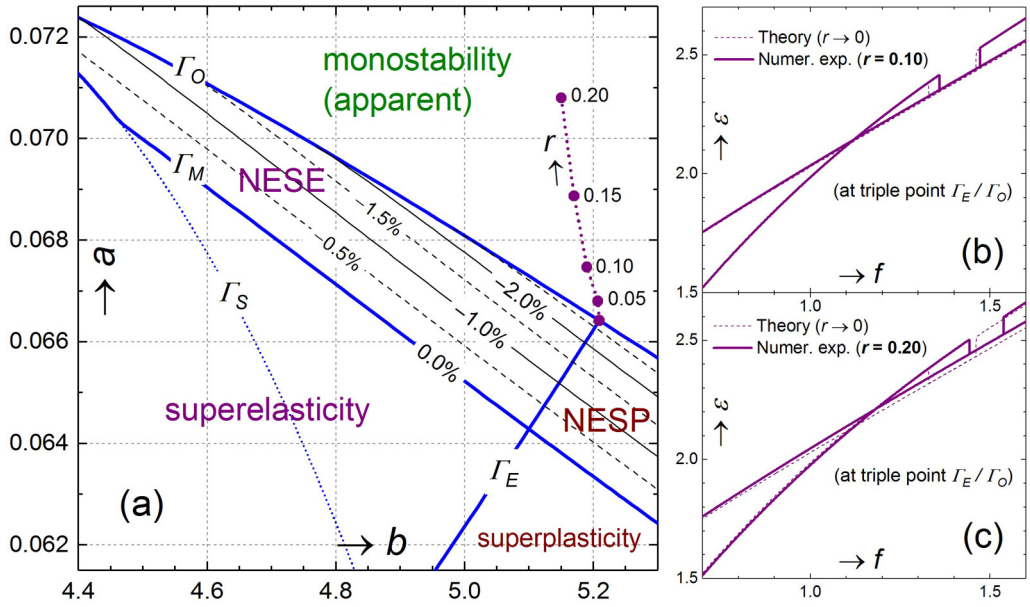

FIG. 9. (a) The vicinity of the NESE, a zoom of the Fig. 8 phase diagram. Shown are the contour lines of the NESE effect intensity defined in (27). The maximal intensity of −2.64% is observed for the triple point ($a = 0.0665$, $b = 5.21$) at the intersection of lines Γ_E and Γ_O. The dotted line marked r shows the drift of this point for a structure, governed by the accurate potential (28), with an increase in the structural aspect ratio $r = H/L$. (b) and (c) Strain-to-load curves of actual structures designed near the triple point at $r = 0.1$ and 0.2, compared to the theoretical prediction discussed in the paper that uses the approximation (4) and corresponds to the limit $r \to 0$.

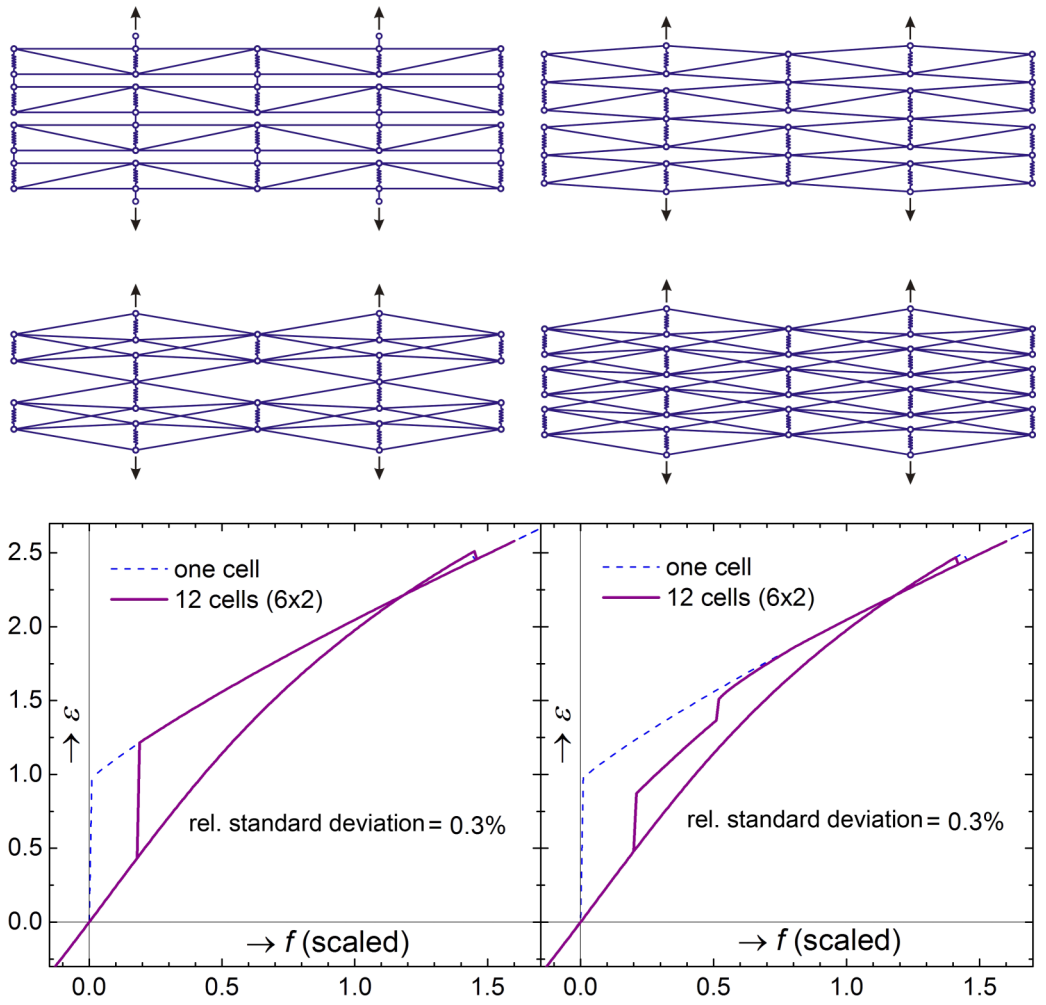

FIG. 10. Possible periodic arrangements of the NESE cells of the Fig. 4 type in a periodic mechanical metamaterial or metastructure. Examples of responses observed in imperfect metastructures of the first type (top left) with random member stiffnesses at a relative standard deviation of 0.3%; $a = 0.0708, b = 5.15, r = 0.2$; periodic boundary conditions are used on the vertical edges, and the loaded nodes are constrained to move synchronically in the vertical direction only; the dashed line is the corresponding single-cell response.

after (x_B) the transition as the following:

$$x_B = x_A(1 + I_{\text{NESE}}). \tag{28}$$

This condition can be used in (26) instead of $x_B = x_A$ to obtain the contour lines corresponding to various fixed values of I_{NESE} with the similar Newton-Raphson iterative procedures. The results are presented in Fig. 9, and we may conclude that the maximal effect should be expected in the vicinity of the triple point formed by the superelasticity (Γ_E) and bistability (Γ_O) boundaries.

Figures 7 and 8 together represent the final phase diagram of the Fig. 4 structure made of five linearly elastic members in terms of the dimensionless system (design) parameters a and b defined in (18). As can be seen, the negative extensibility is a rare behavior occurring only for a small and narrow region in the design space. On the other hand, simplicity of this structure suggests that the negative extensibility is a more ubiquitous property, achievable for a greater range of material systems than previously thought.

V. ERROR ANALYSIS AND OTHER PARAMETERS

In order to understand the error introduced in the analysis with the Green's strain approximation (4), we define an accurate Fig. 4 structure potential using only the engineering strain measure (1),

$$\begin{aligned} \Pi &= \pi_1 + 2(\pi_2 + \pi_3 - Fu), \\ \pi_1 &= \frac{k_1}{2}\left(\sqrt{L^2 + (H - 2v)^2} - \sqrt{L^2 + H^2}\right)^2, \\ \pi_2 &= \frac{k_2}{2}\left(\sqrt{L^2 + (u + v)^2} - L\right)^2, \quad \pi_3 = \frac{k_3}{2}(u + v)^2. \end{aligned} \tag{29}$$

It is more challenging to perform a systematic analysis of this system because a dimensionless form of the potential (29) will require three independent system parameters. Indeed, the mechanical behavior also will depend on the *aspect ratio* of the Fig. 4 structure,

$$r = \frac{H}{L}, \tag{30}$$

and the Fig. 8 diagram will only represent a cross section of the 3D design space of the actual structure at $r \to 0$. Thus, the approximation (4) is good at small aspect ratios when the maximal strain in the bar elements remains low in the hysteretic (bistable) load-unload cycles.

The location of the triple point on the phase diagram representing the maximal NESE effect will drift with r in the hypothetical 3D design space as shown in Fig. 9 with the dashed line. We also found that the greatest discrepancy in the behavior at various $r > 0$'s is seen for the critical (switching) force values, see Figs. 9(b) and 9(c). All other features of the structural response, including the maximal effect intensity are well reproduced for values of r up to 0.30. It is safe to conclude that the approximation (4) and the proposed analysis can provide starting points for a quick search for the negative extensibility or negative compressibility property in the design space of bistable material systems.

The present methodology is also applicable to other accurate potentials of the type (29) without using the approximation (4) when only two variable system parameters can be identified as interesting ones and other parameters are maintained constant. Several successive procedures of this kind could provide useful planar cross sections of the corresponding multidimensional design spaces to identify regions of the negative extensibility behavior. For example, several nonzero values of the *skewness* parameter,

$$s = \frac{h}{H}, \tag{31}$$

of the potential (16) also were considered in the range from -0.5 to 0.5. This parameter was found to have a weak influence on the maximal achievable NESE effect magnitude, although it was slightly better pronounced in rectangular unit cells.

VI. CONCLUSIONS AND OUTLOOKS

We discussed the negative extensibility phenomenon in a simple unit cell structure made of five nonbuckling linearly elastic members, which can be used to fabricate periodic mechanical metamaterials with similar properties. This interesting phenomenon is associated with a special type of bistability transition in the equilibrium solution space of these structures of a more complex type compared to the usual superelastic or superplastic transitions. Simplicity of the unit cell structure studied here suggests that the NESE as a highly interesting property of material systems is probably more ubiquitous than earlier thought. It may exist in simple bistable structures with linear material properties, although a thorough analysis would typically be required to identify the relevant suitable ranges of the design parameters for each system type. Furthermore, caution should be taken to avoid losing this property entirely when attempting to increase the effect intensity by approaching (on the phase diagram) the region of apparent monostability where the bistability is inaccessible in usual load-unload cycles, see Figs. 7 and 8. The reason is the directional nature of negative extensibility property as defined originally in Fig. 1. By mental extension of the contour lines in the Fig. 9 diagram, that region should contain "hidden" negative extensibilities of greater intensities. These behaviors could be unleashed with small additional forces acting on the internal degrees of freedom and making an interesting mechanical device reminiscent of an electronic switch.

Finally, Fig. 10 shows possible arrangements of multiple NESE cells in a periodic metamaterial structure. The collective NESE response of a perfect periodic structure with no randomness in element properties should be equivalent to the unit cell response. However, inevitable small imperfections of elastic member properties in different unit cells may introduce significant deviations from the basic unit cell response. Some of our pilot studies suggest that the critical force value at the NESE transition may shift in both directions, whereas the reverse transition typically shifts toward the center of the hysteresis, and a steplike character of the transitions can also be expected, see Fig. 10. Collective behavior of the bistable periodic NESE medium will certainly have many interesting properties of its own and should be studied more systematically in a separate effort using nonlinear dynamics methods [23,24]. Among these properties are the switching wave propagation speed [25], self-synchronization capabilities, influence of damping components, relaxation transients, effect boundary conditions and loading constraints, and other interesting features. Other simple types of the NESE unit cells should also be sought in the future.

ACKNOWLEDGMENT

This work was supported, in part, by the U.S. National Science Foundation via Grant No. 1634577.

APPENDIX

Analytical solution of Eqs. (22) for the potential (18),

$$f(y,b) = \frac{by(4 - 6y + bP_2)}{2P_1},$$

$$a(y,b) = -\frac{8b(1 - 6y + 6y^2)P_1^2}{27y^2(2 + b - 3by + 2by^2)^2(1 + P_1)^3},$$

$$x(y,b) = \frac{y[12 + 2b(7 - 24y + 18y^2) + 3b^2P_2]}{4P_1}. \tag{A1}$$

Here, the following notations are used:

$$P_1 = 3 + b - 6by + 6by^2,$$
$$P_2 = 1 - 9y + 26y^2 - 30y^3 + 12y^4. \tag{A2}$$

[1] R. S. Lakes, Foam structures with a negative Poisson's ratio, Science **235**, 1038 (1987).

[2] M. I. Hussein, D. Torrent, and O. R. Bilal, Editorial for the focus issue on Frontiers of Mechanical Metamaterials, Extreme Mech. Lett. **12**, 1 (2017).

[3] E. G. Karpov, Structural metamaterials with Saint-Venant edge effect reversal, Acta Mater. **123**, 245 (2017).

[4] F. Scarpa and P. J. Tomlin, On the transverse shear modulus of negative Poisson's ratio honeycomb structures, Fatigue Fract. Eng. Mater. Struct. **23**, 717 (2000).

[5] J. N. Grima, R. Caruana-Gauci, K. W. Wojciechowski, and K. E. Evans, Smart hexagonal truss systems exhibiting negative compressibility through constrained angle stretching, Smart Mater. Structures **22**, 084015 (2013).
[6] W. Yang, Z. M. Li, W. Shi, B. H. Xie, and M. B. Yang, Review on auxetic materials, J. Mater. Sci. **39**, 3269 (2004).
[7] J. W. Jiang and H. S. Park, Negative Poisson's ratio in single-layer black phosphorus, Nat. Commun. **5**, 4727 (2014).
[8] T. C. Lim, *Auxetic Materials and Structures* (Springer, Berlin, 2015).
[9] J. W. Jiang, S. Y. Kim, and H. S. Park, Auxetic nanomaterials: Recent progress and future development, Appl. Phys. Rev. **3**, 041101 (2016).
[10] M. Schenk and S. D. Guest, Geometry of Miura-Folded Metamaterials, Proc. Natl. Acad. Sci. USA **110**, 3276 (2013).
[11] Z. Y. Wei, Z. V. Guo, L. Dudte, H. Y. Liang, and L. Mahadevan, Geometric Mechanics of Periodic Pleated Origami, Phys. Rev. Lett. **110**, 215501 (2013).
[12] J. L. Silverberg, A. A. Evans, L. McLeod, R. C. Hayward, T. Hull, C. D. Santangelo, and I. Cohen, Using origami design principles to fold reprogrammable mechanical metamaterials, Science **345**, 647 (2014).
[13] S. Shan, S. Kang, Z. Zhao, L. Fang, and K. Bertoldi, Design of planar isotropic negative Poisson's ratio structures, Extreme Mech. Lett. **4**, 96 (2015).
[14] S. Shan, S. Kang, J. R. Raney, P. Wang, L. Fang, F. Candido, J. A. Lewis, and K. Bertoldi, Multistable architected materials for trapping elastic strain energy, Adv. Mater. **27**, 4296 (2015).
[15] Z. G. Nicolaou and A. E. Motter, Mechanical metamaterials with negative compressibility transitions, Nature Mater. **11**, 608 (2012).
[16] Z. G. Nicolaou and A. E. Motter, Longitudinal inverted compressibility in super-strained metamaterials, J. Stat. Phys. **151**, 1162 (2013).
[17] M. L. Chen and E. G. Karpov, Bistability and thermal coupling in elastic metamaterials with negative compressibility, Phys. Rev. E **90**, 033201 (2014).
[18] C. Coulais, D. Sounas, and A. Alu, Static non-reciprocity in mechanical metamaterials, Nature (London) **542**, 461 (2017).
[19] R. Gilmore, *Catastrophe Theory for Scientists and Engineers* (Wiley, New York, 1981).
[20] P. T. Saunders, *An Introduction to Catastrophe Theory* (Cambridge University Press, Cambridge, UK, 1986).
[21] V. I. Arnold, *Catastrophe Theory* (Springer-Verlag, Berlin, 1992).
[22] L. A. Danso and E. G. Karpov, Cusp singularity-based bistability criterion for geometrically nonlinear structures, Extreme Mech. Lett. **13**, 135 (2017).
[23] S. H. Strogatz, *Nonlinear Dynamics and Chaos: With Applications to Physics, Biology, Chemistry, and Engineering* (Westview, Boulder, CO, 2001).
[24] E. G. Karpov, Bistability, autowaves and dissipative structures in semiconductor fibers with anomalous resistivity properties, Philos. Mag. **92**, 1300 (2012).